

Observation of Electron Neutrino Appearance in a Muon Neutrino Beam

K. Abe,⁴⁶ J. Adam,³² H. Aihara,^{45,23} T. Akiri,⁹ C. Andreopoulos,⁴⁴ S. Aoki,²⁴ A. Ariga,² T. Ariga,² S. Assylbekov,⁸ D. Autiero,²⁹ M. Barbi,³⁹ G.J. Barker,⁵⁴ G. Barr,³⁵ M. Bass,⁸ M. Batkiewicz,¹³ F. Bay,¹¹ S.W. Bentham,²⁶ V. Berardi,¹⁸ B.E. Berger,⁸ S. Berkman,⁴ I. Bertram,²⁶ S. Bhadra,⁵⁸ F.d.M. Blaszczyk,²⁸ A. Blondel,¹² C. Bojecho,⁵¹ S. Bordoni,¹⁵ S.B. Boyd,⁵⁴ D. Brailsford,¹⁷ A. Bravar,¹² C. Bronner,²⁵ N. Buchanan,⁸ R.G. Calland,²⁷ J. Caravaca Rodríguez,¹⁵ S.L. Cartwright,⁴² R. Castillo,¹⁵ M.G. Catanesi,¹⁸ A. Cervera,¹⁶ D. Cherdack,⁸ G. Christodoulou,²⁷ A. Clifton,⁸ J. Coleman,²⁷ S.J. Coleman,⁷ G. Collazuol,²⁰ K. Connolly,⁵⁵ L. Cremonesi,³⁸ A. Dabrowska,¹³ I. Danko,³⁷ R. Das,⁸ S. Davis,⁵⁵ P. de Perio,⁴⁹ G. De Rosa,¹⁹ T. Dealtry,^{44,35} S.R. Dennis,^{54,44} C. Densham,⁴⁴ F. Di Lodovico,³⁸ S. Di Luise,¹¹ O. Drapier,¹⁰ T. Duboyski,³⁸ K. Duffy,³⁵ F. Dufour,¹² J. Dumarchez,³⁶ S. Dytman,³⁷ M. Dziewiecki,⁵³ S. Emery,⁶ A. Ereditato,² L. Escudero,¹⁶ A.J. Finch,²⁶ L. Floetotto,⁴¹ M. Friend,^{14,*} Y. Fujii,^{14,*} Y. Fukuda,³⁰ A.P. Furmanski,⁵⁴ V. Galymov,⁶ A. Gaudin,⁵¹ S. Giffin,³⁹ C. Giganti,³⁶ K. Gilje,³² D. Goeldi,² T. Golan,⁵⁷ J.J. Gomez-Cadenas,¹⁶ M. Gonin,¹⁰ N. Grant,²⁶ D. Gudin,²² D.R. Hadley,⁵⁴ A. Haesler,¹² M.D. Haigh,⁵⁴ P. Hamilton,¹⁷ D. Hansen,³⁷ T. Hara,²⁴ M. Hartz,^{23,50} T. Hasegawa,^{14,*} N.C. Hastings,³⁹ Y. Hayato,⁴⁶ C. Hearty,^{4,†} R.L. Helmer,⁵⁰ M. Hierholzer,² J. Hignight,³² A. Hillairet,⁵¹ A. Himmel,⁹ T. Hiraki,²⁵ S. Hirota,²⁵ J. Holeczek,⁴³ S. Horikawa,¹¹ K. Huang,²⁵ A.K. Ichikawa,²⁵ K. Ieki,²⁵ M. Ieva,¹⁵ M. Ikeda,⁴⁶ J. Imber,³² J. Insler,²⁸ T.J. Irvine,⁴⁷ T. Ishida,^{14,*} T. Ishii,^{14,*} S.J. Ives,¹⁷ K. Iyogi,⁴⁶ A. Izmaylov,^{16,22} A. Jacob,³⁵ B. Jamieson,⁵⁶ R.A. Johnson,⁷ J.H. Jo,³² P. Jonsson,¹⁷ C.K. Jung,^{32,‡} A.C. Kaboth,¹⁷ T. Kajita,^{47,‡} H. Kakuno,⁴⁸ J. Kameda,⁴⁶ Y. Kanazawa,⁴⁵ D. Karlen,^{51,50} I. Karpikov,²² E. Kearns,^{3,23,‡} M. Khabibullin,²² A. Khotjantsev,²² D. Kielczewska,⁵² T. Kikawa,²⁵ A. Kilinski,³¹ J. Kim,⁴ J. Kisiel,⁴³ P. Kitching,¹ T. Kobayashi,^{14,*} L. Koch,⁴¹ A. Kolaceke,³⁹ A. Konaka,⁵⁰ L.L. Kormos,²⁶ A. Korzenev,¹² K. Koseki,^{14,*} Y. Koshio,^{33,‡} I. Kreslo,² W. Kropp,⁵ H. Kubo,²⁵ Y. Kudenko,^{22,§} S. Kumaratunga,⁵⁰ R. Kurjata,⁵³ T. Kutter,²⁸ J. Lagoda,³¹ K. Laihem,⁴¹ I. Lamont,²⁶ M. Laveder,²⁰ M. Lawe,⁴² M. Lazos,²⁷ K.P. Lee,⁴⁷ C. Licciardi,³⁹ T. Lindner,⁵⁰ C. Lister,⁵⁴ R.P. Litchfield,⁵⁴ A. Longhin,²⁰ L. Ludovici,²¹ M. Macaire,⁶ L. Magaletti,¹⁸ K. Mahn,⁵⁰ M. Malek,¹⁷ S. Manly,⁴⁰ A.D. Marino,⁷ J. Marteau,²⁹ J.F. Martin,⁴⁹ T. Maruyama,^{14,*} J. Marzec,⁵³ E.L. Mathie,³⁹ V. Matveev,²² K. Mavrokoridis,²⁷ E. Mazzucato,⁶ M. McCarthy,⁴ N. McCauley,²⁷ K.S. McFarland,⁴⁰ C. McGrew,³² C. Metelko,²⁷ M. Mezzetto,²⁰ P. Mijakowski,³¹ C.A. Miller,⁵⁰ A. Minamino,²⁵ O. Mineev,²² S. Mine,⁵ A. Missert,⁷ M. Miura,^{46,‡} L. Monfregola,¹⁶ S. Moriyama,^{46,‡} Th.A. Mueller,¹⁰ A. Murakami,²⁵ M. Murdoch,²⁷ S. Murphy,¹¹ J. Myslik,⁵¹ T. Nagasaki,²⁵ T. Nakadaira,^{14,*} M. Nakahata,^{46,23} T. Nakai,³⁴ K. Nakamura,^{23,14,*} S. Nakayama,^{46,‡} T. Nakaya,^{25,23} K. Nakayoshi,^{14,*} D. Naples,³⁷ C. Nielsen,⁴ M. Nirkko,² K. Nishikawa,^{14,*} Y. Nishimura,⁴⁷ H.M. O'Keefe,²⁶ R. Ohta,^{14,*} K. Okumura,^{47,23} T. Okusawa,³⁴ W. Orszyszczak,⁵² S.M. Oser,⁴ R.A. Owen,³⁸ Y. Oyama,^{14,*} V. Palladino,¹⁹ V. Paolone,³⁷ D. Payne,²⁷ G.F. Pearce,⁴⁴ O. Perevozchikov,²⁸ J.D. Perkin,⁴² Y. Petrov,⁴ L.J. Pickard,⁴² E.S. Pinzon Guerra,⁵⁸ C. Pistillo,² P. Plonski,⁵³ E. Poplawska,³⁸ B. Popov,^{36,¶} M. Posiadala,⁵² J.-M. Poutissou,⁵⁰ R. Poutissou,⁵⁰ P. Przewlocki,³¹ B. Quilain,¹⁰ E. Radicioni,¹⁸ P.N. Ratoff,²⁶ M. Ravonel,¹² M.A.M. Rayner,¹² A. Redij,² M. Reeves,²⁶ E. Reinherz-Aronis,⁸ F. Retiere,⁵⁰ A. Robert,³⁶ P.A. Rodrigues,⁴⁰ P. Rojas,⁸ E. Rondio,³¹ S. Roth,⁴¹ A. Rubbia,¹¹ D. Ruterbories,⁸ R. Sacco,³⁸ K. Sakashita,^{14,*} F. Sánchez,¹⁵ F. Sato,¹⁴ E. Scantamburlo,¹² K. Scholberg,^{9,‡} J. Schwehr,⁸ M. Scott,⁵⁰ Y. Seiya,³⁴ T. Sekiguchi,^{14,*} H. Sekiya,^{46,‡} D. Sgalaberna,¹¹ M. Shiozawa,^{46,23} S. Short,¹⁷ Y. Shustrov,²² P. Sinclair,¹⁷ B. Smith,¹⁷ R.J. Smith,³⁵ M. Smy,⁵ J.T. Sobczyk,⁵⁷ H. Sobel,^{5,23} M. Sorel,¹⁶ L. Southwell,²⁶ P. Stamoulis,¹⁶ J. Steinmann,⁴¹ B. Still,³⁸ Y. Suda,⁴⁵ A. Suzuki,²⁴ K. Suzuki,²⁵ S.Y. Suzuki,^{14,*} Y. Suzuki,^{46,23} T. Szegowski,⁴³ R. Tacik,^{39,50} M. Tada,^{14,*} S. Takahashi,²⁵ A. Takeda,⁴⁶ Y. Takeuchi,^{24,23} H.K. Tanaka,^{46,‡} H.A. Tanaka,^{4,†} M.M. Tanaka,^{14,*} D. Terhorst,⁴¹ R. Terri,³⁸ L.F. Thompson,⁴² A. Thorley,²⁷ S. Tobayama,⁴ W. Toki,⁸ T. Tomura,⁴⁶ Y. Totsuka,^{**} C. Touramanis,²⁷ T. Tsukamoto,^{14,*} M. Tzanov,²⁸ Y. Uchida,¹⁷ K. Ueno,⁴⁶ A. Vacheret,³⁵ M. Vagins,^{23,5} G. Vasseur,⁶ T. Wachala,¹³ A.V. Waldron,³⁵ C.W. Walter,^{9,‡} D. Wark,^{44,17} M.O. Wascko,¹⁷ A. Weber,^{44,35} R. Wendell,^{46,‡} R.J. Wilkes,⁵⁵ M.J. Wilking,⁵⁰ C. Wilkinson,⁴² Z. Williamson,³⁵ J.R. Wilson,³⁸ R.J. Wilson,⁸ T. Wongjirad,⁹ Y. Yamada,^{14,*} K. Yamamoto,³⁴ C. Yanagisawa,^{32,††} S. Yen,⁵⁰ N. Yershov,²² M. Yokoyama,^{45,‡} T. Yuan,⁷ A. Zalewska,¹³ J. Zalipska,³¹ L. Zambelli,³⁶ K. Zaremba,⁵³ M. Ziembicki,⁵³ E.D. Zimmerman,⁷ M. Zito,⁶ and J. Żmuda⁵⁷

(The T2K Collaboration)

¹University of Alberta, Centre for Particle Physics, Department of Physics, Edmonton, Alberta, Canada

²University of Bern, Albert Einstein Center for Fundamental Physics,
Laboratory for High Energy Physics (LHEP), Bern, Switzerland

³Boston University, Department of Physics, Boston, Massachusetts, U.S.A.

- ⁴University of British Columbia, Department of Physics and Astronomy, Vancouver, British Columbia, Canada
- ⁵University of California, Irvine, Department of Physics and Astronomy, Irvine, California, U.S.A.
- ⁶IRFU, CEA Saclay, Gif-sur-Yvette, France
- ⁷University of Colorado at Boulder, Department of Physics, Boulder, Colorado, U.S.A.
- ⁸Colorado State University, Department of Physics, Fort Collins, Colorado, U.S.A.
- ⁹Duke University, Department of Physics, Durham, North Carolina, U.S.A.
- ¹⁰Ecole Polytechnique, IN2P3-CNRS, Laboratoire Leprince-Ringuet, Palaiseau, France
- ¹¹ETH Zurich, Institute for Particle Physics, Zurich, Switzerland
- ¹²University of Geneva, Section de Physique, DPNC, Geneva, Switzerland
- ¹³H. Niewodniczanski Institute of Nuclear Physics PAN, Cracow, Poland
- ¹⁴High Energy Accelerator Research Organization (KEK), Tsukuba, Ibaraki, Japan
- ¹⁵Institut de Fisica d'Altes Energies (IFAE), Bellaterra (Barcelona), Spain
- ¹⁶IFIC (CSIC & University of Valencia), Valencia, Spain
- ¹⁷Imperial College London, Department of Physics, London, United Kingdom
- ¹⁸INFN Sezione di Bari and Università e Politecnico di Bari, Dipartimento Interuniversitario di Fisica, Bari, Italy
- ¹⁹INFN Sezione di Napoli and Università di Napoli, Dipartimento di Fisica, Napoli, Italy
- ²⁰INFN Sezione di Padova and Università di Padova, Dipartimento di Fisica, Padova, Italy
- ²¹INFN Sezione di Roma and Università di Roma "La Sapienza", Roma, Italy
- ²²Institute for Nuclear Research of the Russian Academy of Sciences, Moscow, Russia
- ²³Kavli Institute for the Physics and Mathematics of the Universe (WPI),
Todai Institutes for Advanced Study, University of Tokyo, Kashiwa, Chiba, Japan
- ²⁴Kobe University, Kobe, Japan
- ²⁵Kyoto University, Department of Physics, Kyoto, Japan
- ²⁶Lancaster University, Physics Department, Lancaster, United Kingdom
- ²⁷University of Liverpool, Department of Physics, Liverpool, United Kingdom
- ²⁸Louisiana State University, Department of Physics and Astronomy, Baton Rouge, Louisiana, U.S.A.
- ²⁹Université de Lyon, Université Claude Bernard Lyon 1, IPN Lyon (IN2P3), Villeurbanne, France
- ³⁰Miyagi University of Education, Department of Physics, Sendai, Japan
- ³¹National Centre for Nuclear Research, Warsaw, Poland
- ³²State University of New York at Stony Brook, Department of Physics and Astronomy, Stony Brook, New York, U.S.A.
- ³³Okayama University, Department of Physics, Okayama, Japan
- ³⁴Osaka City University, Department of Physics, Osaka, Japan
- ³⁵Oxford University, Department of Physics, Oxford, United Kingdom
- ³⁶UPMC, Université Paris Diderot, CNRS/IN2P3, Laboratoire de
Physique Nucléaire et de Hautes Energies (LPNHE), Paris, France
- ³⁷University of Pittsburgh, Department of Physics and Astronomy, Pittsburgh, Pennsylvania, U.S.A.
- ³⁸Queen Mary University of London, School of Physics and Astronomy, London, United Kingdom
- ³⁹University of Regina, Department of Physics, Regina, Saskatchewan, Canada
- ⁴⁰University of Rochester, Department of Physics and Astronomy, Rochester, New York, U.S.A.
- ⁴¹RWTH Aachen University, III. Physikalisches Institut, Aachen, Germany
- ⁴²University of Sheffield, Department of Physics and Astronomy, Sheffield, United Kingdom
- ⁴³University of Silesia, Institute of Physics, Katowice, Poland
- ⁴⁴STFC, Rutherford Appleton Laboratory, Harwell Oxford, and Daresbury Laboratory, Warrington, United Kingdom
- ⁴⁵University of Tokyo, Department of Physics, Tokyo, Japan
- ⁴⁶University of Tokyo, Institute for Cosmic Ray Research, Kamioka Observatory, Kamioka, Japan
- ⁴⁷University of Tokyo, Institute for Cosmic Ray Research, Research Center for Cosmic Neutrinos, Kashiwa, Japan
- ⁴⁸Tokyo Metropolitan University, Department of Physics, Tokyo, Japan
- ⁴⁹University of Toronto, Department of Physics, Toronto, Ontario, Canada
- ⁵⁰TRIUMF, Vancouver, British Columbia, Canada
- ⁵¹University of Victoria, Department of Physics and Astronomy, Victoria, British Columbia, Canada
- ⁵²University of Warsaw, Faculty of Physics, Warsaw, Poland
- ⁵³Warsaw University of Technology, Institute of Radioelectronics, Warsaw, Poland
- ⁵⁴University of Warwick, Department of Physics, Coventry, United Kingdom
- ⁵⁵University of Washington, Department of Physics, Seattle, Washington, U.S.A.
- ⁵⁶University of Winnipeg, Department of Physics, Winnipeg, Manitoba, Canada
- ⁵⁷Wroclaw University, Faculty of Physics and Astronomy, Wroclaw, Poland
- ⁵⁸York University, Department of Physics and Astronomy, Toronto, Ontario, Canada

(Dated: April 17, 2014)

The T2K experiment has observed electron neutrino appearance in a muon neutrino beam produced 295 km from the Super-Kamiokande detector with a peak energy of 0.6 GeV. A total of 28 electron neutrino events were detected with an energy distribution consistent with an appearance signal, corresponding to a significance of 7.3σ when compared to 4.92 ± 0.55 expected background events. In the PMNS mixing model, the electron neutrino appearance signal depends on several

parameters including three mixing angles θ_{12} , θ_{23} , θ_{13} , a mass difference Δm_{32}^2 and a CP violating phase δ_{CP} . In this neutrino oscillation scenario, assuming $|\Delta m_{32}^2| = 2.4 \times 10^{-3} \text{ eV}^2$, $\sin^2 \theta_{23} = 0.5$, and $\Delta m_{32}^2 > 0$ ($\Delta m_{32}^2 < 0$), a best-fit value of $\sin^2 2\theta_{13} = 0.140_{-0.032}^{+0.038}$ ($0.170_{-0.037}^{+0.045}$) is obtained at $\delta_{\text{CP}} = 0$. When combining the result with the current best knowledge of oscillation parameters including the world average value of θ_{13} from reactor experiments, some values of δ_{CP} are disfavored at the 90% CL.

PACS numbers: 14.60.Pq, 14.60.Lm, 25.30.Pt, 29.40.Ka

Introduction—The discovery of neutrino oscillations using atmospheric neutrinos was made by Super-Kamiokande in 1998 [1]. Since then, many other experiments have confirmed the phenomenon of neutrino oscillations through various disappearance modes of flavor transformations. However, to date, there has not been an observation of the explicit appearance of a different neutrino flavor from neutrinos of another flavor through neutrino oscillations. In 2011, the T2K collaboration published the first indication of electron neutrino appearance from a muon neutrino beam at 2.5σ significance based on a data set corresponding to 1.43×10^{20} protons on target (POT) [2, 3]. This result was followed by the publication of further evidence for electron neutrino appearance at 3.1σ in early 2013 [4]. This paper presents new results from the T2K experiment that establish, at greater than 5σ , the observation of electron-neutrino appearance from a muon-neutrino beam.

In a three-flavor framework, neutrino oscillations are described by the PMNS matrix [5, 6] which is parameterized by three mixing angles θ_{12} , θ_{23} , θ_{13} , and a CP violating phase δ_{CP} . In this framework the probability for $\nu_\mu \rightarrow \nu_e$ oscillation can be expressed [7] as

$$P(\nu_\mu \rightarrow \nu_e) \simeq \sin^2 \theta_{23} \sin^2 2\theta_{13} \sin^2 \frac{\Delta m_{31}^2 L}{4E} - \frac{\sin 2\theta_{12} \sin 2\theta_{23}}{2 \sin \theta_{13}} \sin \frac{\Delta m_{21}^2 L}{4E} \sin^2 2\theta_{13} \sin^2 \frac{\Delta m_{31}^2 L}{4E} \sin \delta_{\text{CP}} + (\text{CP even term, solar term, matter effect term}), \quad (1)$$

where L is the neutrino propagation distance and E is the neutrino energy. The measurement of $\nu_\mu \rightarrow \nu_e$ oscillations is of particular interest because this mode is sensitive to both θ_{13} and δ_{CP} . The first indication of non-zero θ_{13} was published by T2K [3] based on the measurement of $\nu_\mu \rightarrow \nu_e$ oscillations. More recently, indications of $\nu_\mu \rightarrow \nu_e$ oscillations were also reported by the MINOS experiment [12]. The value of θ_{13} is now precisely known to be $9.1 \pm 0.6^\circ$ from measurements of $\bar{\nu}_e$ disappearance in reactor neutrino experiments [8–11]. Using the reactor measurement of θ_{13} , the $\nu_\mu \rightarrow \nu_e$ appearance mode can be used to explore CP violation, which has yet to be observed in the lepton sector. CP violation, as shown in Equation 1, is governed by the second term and can be as large as 27% of the first term for the T2K experimental setup when using current values of the neutrino oscillation parameters.

T2K Experiment—T2K operates at the J-PARC facility in Tokai, Japan. A muon neutrino beam is produced

from the decay of charged pions and kaons generated by 30 GeV protons hitting a graphite target and focused by three magnetic horns. Downstream of the horns is the decay volume, 96 meters in length, followed by the beam dump and muon monitors (MUMON). The neutrino beam illuminates an on-axis detector and off-axis detectors positioned at an angle of 2.5° relative to the beam direction. The resulting energy spectrum, peaked at 0.6 GeV for the off-axis detectors, reduces the ν_e contamination and the feed-down backgrounds to the ν_e appearance signal from higher energy neutrinos. The near detector complex at 280 meters from the target is used to measure the neutrino beam direction, spectrum, and composition before oscillations and to measure neutrino cross sections. The complex consists of an on-axis detector (INGRID) and a suite of off-axis detectors (ND280) that reside within a 0.2 T magnet [2]. The Super-Kamiokande (SK) 50 kt water Cherenkov detector, situated 295 km away, is used to detect the oscillated neutrinos.

The results presented here are based on data taken from January 2010 to May 2013. During this period the proton beam power has steadily increased and reached 220 kW continuous operation with a world record of 1.2×10^{14} protons per pulse. The total neutrino beam exposure at SK corresponds to 6.57×10^{20} POT.

Neutrino Beam Flux—The neutrino beam flux [13] is predicted by modeling interactions of the primary beam protons in a graphite target using external hadron production data from the CERN NA61/SHINE experiment [14, 15] and the FLUKA2008 package [16, 17]. GEANT3 [18] with GCALOR [19] simulates propagation of the secondary/tertiary pions and kaons, and their decays into neutrinos. The ν_e component (including a small amount of $\bar{\nu}_e$) in the beam is estimated to be less than 1% of the flux below 1.5 GeV, and constitutes an irreducible background to the ν_e appearance search. This component is generated predominantly by the decay of muons for $E_\nu < 1$ GeV and by kaons for $E_\nu > 1$ GeV.

The neutrino flux uncertainties are dominated by the hadron production uncertainties, with contributions from the neutrino beam direction and the proton beam uncertainties. The neutrino beam direction, monitored indirectly by MUMON on a spill-by-spill basis, and directly by INGRID [20], was found to be well within the required ± 1 mrad during the full run period. INGRID also measured the neutrino interaction rate per POT to be stable

within 0.7%. The total systematic error for the absolute flux prediction is evaluated to be 10–15% in the relevant energy range. Furthermore, the uncertainty on the ratio of the flux predictions at the far and the near detectors is less than 2% around the peak.

Neutrino Interaction Simulations and Cross Section Parameters—The NEUT neutrino interaction generator [21] is used to simulate neutrino interactions in the INGRID, ND280, and SK detectors. At interaction energies typical of the T2K beam, the dominant charged current (CC) interactions are charged current quasi-elastic (CCQE) and single resonant pion production. The cross section parameterization can be divided into two categories: parameters common to interactions at both ND280 and SK, and parameters evaluated separately for the two detectors. Parameters in the first category comprise the axial masses for CCQE (M_A^{QE}) and single resonant pion production (M_A^{RES}), and normalizations for CCQE, CC single pion, and neutral current (NC) $1\pi^0$ interactions. Parameters in the second category are typically related to the interaction target—primarily carbon at ND280 and oxygen at SK—and include Fermi momentum, binding energy, and spectral function modeling for the CCQE nuclear model. Also in this category are normalizations for other CC and NC cross sections, the ν_e/ν_μ CC cross section ratio, pion production parameters, and final state interactions of pions exiting the nucleus. External data sets, primarily from [22–24], are used to determine the initial values and prior uncertainties of the parameters [4].

ND280 Measurements, Flux and Common Cross Section fits—The energy spectrum of the neutrino beam and the neutrino cross section parameters are constrained using ν_μ CC interactions in ND280. The fine-grained detectors (FGDs) [25] are scintillator trackers that serve as the primary neutrino target, and the momentum and identity of the particles emerging from the interaction are determined by the time projection chambers (TPCs) [26] interleaved with the FGDs. The muon is assumed to be the highest-momentum, negative-curvature track that emerges from the FGD fiducial volume with an energy deposition consistent with a muon in the TPC downstream of the FGD. Tracks found in the TPC upstream of the FGD are used to veto external background events.

The ND280 analysis includes many improvements over the previous T2K electron neutrino appearance measurement [4]. Candidate events are now divided into three samples: CC- 0π , dominated by CCQE interactions; CC- $1\pi^+$, dominated by CC resonant pion production; and CC-other. The samples are defined by the number of pions in the observed final state. A π^+ can be identified in one of three ways: an FGD+TPC track with positive curvature and a TPC charge deposition consistent with a pion, an FGD-contained track with a charge deposition consistent with a pion, or a delayed energy deposit due to a decay electron from stopped $\pi^+ \rightarrow \mu^+$ in the FGD.

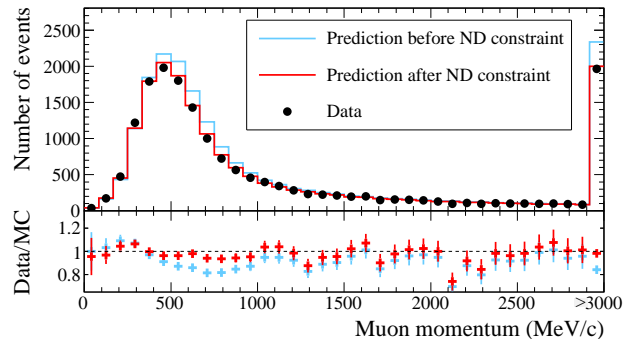


FIG. 1. The muon momentum distribution for the ND280 CC- 0π sample (upper). The black points represent the data, the blue histogram shows the MC prediction before data constraint, and the red histogram shows the MC prediction after constraint. The lower plot shows the ratio of data to MC for the pre- and post-constraint cases.

To tag a π^- , only negative curvature FGD+TPC tracks are used. A π^0 is identified if there exists a track in the TPC with a charge deposition consistent with an electron from a γ conversion. Events containing no pions are classified as CC- 0π , events with exactly one π^+ and no π^- or π^0 are classified as CC- $1\pi^+$, and all other CC events are classified as CC-other. There are 17369, 4047, and 4173 data events in the CC- 0π , CC- $1\pi^+$, and CC-other samples, respectively. The ND280 data set used for this analysis corresponds to 5.90×10^{20} POT.

The three samples are fit with 25 beam flux parameters at ND280 (11 E_{ν_μ} , 5 $E_{\bar{\nu}_\mu}$, 7 E_{ν_e} , and 2 $E_{\bar{\nu}_e}$ bins), 21 cross section parameters (5 in common with SK, and 16 used only for ND280), as well as 210 parameters describing the ND280 detector systematics (10 momentum \times 7 angle bins for each sample). The dominant detector uncertainties come from events occurring outside the FGD fiducial volume and from pion reinteractions in the detector. The ND280 measurements constrain the SK flux parameters due to the flux covariance derived from beam simulations. The predicted numbers of ND280 events in Monte Carlo (MC), using the best-fit parameters, are 17352, 4110, and 4119 for the CC- 0π , CC- $1\pi^+$, and CC-other samples, respectively. A χ^2 goodness-of-fit test returns a p-value of 0.66, indicating no disagreement between the data and the prediction using best-fit parameters. Figure 1 shows the muon momentum distribution of the CC- 0π sample, and the improvement in data and MC agreement when using the best-fit parameters.

The fit to the ND280 data gives estimates for 22 beam flux parameters at SK, the 5 common cross section parameters, and their covariance. Using the ND280 information reduces the uncertainty on the expected number of electron-like events at SK due to the propagated parameters from 25.9% to 2.9%.

SK Measurements—The SK detector is composed of

an inner detector (ID) and an outer detector (OD). The ID has a water fiducial volume (FV) of 22.5 kt that is equipped with 11129 photomultiplier tubes (PMT) and is surrounded by the 2 m wide OD. Neutrino events at SK are selected if the Cherenkov ring is consistent with an energy above 30 MeV in the ID with low activity in the OD to reject any entering background or exiting events. These events are labeled fully-contained (FC). The FC fiducial volume (FCFV) sample is obtained by applying the further cut that the event vertex is at least 2 m away from the ID tank wall. A timing cut of -2 to $10 \mu\text{s}$ relative to the first beam bunch arrival is applied to distinguish T2K data from other neutrino samples such as atmospheric neutrino interactions. The timing cut reduces the contamination from other neutrino sources to 0.0085 events in the full sample.

To select ν_e interaction candidate events in the FCFV sample, a single electron-like Cherenkov ring is required. The reconstructed electron momentum (p_e) is required to exceed 100 MeV/c to eliminate decay-electrons from stopping muons generated by CC interactions and pions in NC interactions. In addition, events are required to have a reconstructed neutrino energy (E_ν^{rec}) below 1250 MeV. Nearly all of the oscillated ν_e signal events are below this value, while most of the intrinsic beam ν_e background events have higher energies. The E_ν^{rec} is calculated assuming a CCQE interaction as

$$E_\nu^{\text{rec}} = \frac{m_p^2 - (m_n - E_b)^2 - m_e^2 + 2(m_n - E_b)E_e}{2(m_n - E_b - E_e + p_e \cos \theta_e)}, \quad (2)$$

where m_n (m_p) is the neutron (proton) mass, E_b is the neutron binding energy in oxygen (27 MeV), m_e is the electron mass, E_e is its energy, and θ_e is the angle of the electron direction relative to the beam direction.

The final selection criterion removes additional π^0 background events using a new reconstruction algorithm, based on an extension of the model described in Reference [27], to determine the kinematics of all final state particles. The new algorithm is a maximum-likelihood fit in which charge and time probability density functions (PDFs) are constructed for every PMT hit for a given particle hypothesis with a set of 7 parameters: the vertex position, the timing, the direction and the momentum. Multiple-particle fit hypotheses are constructed by summing the charge contributions from each constituent particle. Different neutrino final states are distinguished by comparing the best-fit likelihood resulting from the fit of each hypothesis. To separate π^0 events from ν_e CC events, both the reconstructed π^0 mass (m_{π^0}) and the ratio of the best-fit likelihoods of the π^0 and electron fits (L_{π^0}/L_e) are used. Figure 2 shows the $\ln(L_{\pi^0}/L_e)$ vs π^0 mass distribution for signal ν_e -CC events and events containing a π^0 in the MC sample, as well as the rejection cut line. Events that satisfy $\ln(L_{\pi^0}/L_e) < 175 - 0.875 \times m_{\pi^0}$ (MeV/c²) constitute the final ν_e candidate sample. This cut removes 69% of

the π^0 background events relative to the previous T2K ν_e appearance selection, with only a 2% loss in signal efficiency [3].

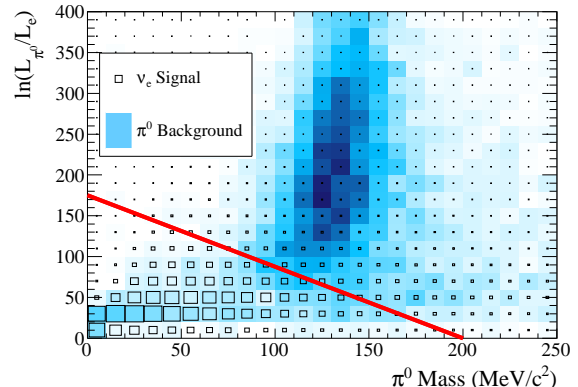


FIG. 2. The $\ln(L_{\pi^0}/L_e)$ vs m_{π^0} distribution is shown for both signal ν_e -CC events (boxes) and background events containing a π^0 (blue scale). The red line indicates the location of the π^0 rejection cut. Events in the upper right corner are rejected.

A summary of the number of events passing each selection cut is shown in Table I. After all cuts, the total number of candidate ν_e events selected in data is 28, which is significantly larger than the 4.92 ± 0.55 expected events for $\theta_{13} = 0$. For $\sin^2 2\theta_{13} = 0.1$ and $\delta_{\text{CP}} = 0$, the expected number is 21.6, as shown in Table I.

TABLE I. The expected number of signal and background events passing each selection stage assuming $\sin^2 2\theta_{13} = 0.1$, $\sin^2 \theta_{23} = 0.5$, $|\Delta m_{32}^2| = 2.4 \times 10^{-3} \text{ eV}^2$, $\delta_{\text{CP}} = 0$, and $\Delta m_{32}^2 > 0$, compared to the observed number in data. Interactions in the true FV are based on the MC truth information while all other numbers are based on the reconstructed information and have been rounded off after addition to avoid rounding error.

Selection	Data	$\nu_\mu \rightarrow \nu_e$	$\nu_\mu + \bar{\nu}_\mu$	$\nu_e + \bar{\nu}_e$	NC	Total MC
		CC	CC	CC		
Interactions in FV	-	27.1	325.7	16.0	288.1	656.8
FCFV	377	26.2	247.8	15.4	83.0	372.4
+Single-ring	193	22.7	142.4	9.8	23.5	198.4
+e-like PID	60	22.4	5.6	9.7	16.3	54.2
+ $p_e > 100 \text{ MeV/c}$	57	22.0	3.7	9.7	14.0	49.4
+No decay-e	44	19.6	0.7	7.9	11.8	40.0
+ $E_\nu^{\text{rec}} < 1250 \text{ MeV}$	39	18.8	0.2	3.7	9.0	31.7
+Non- π^0 -like	28	17.3	0.1	3.2	1.0	21.6

The systematic uncertainty due to the SK selection cuts is evaluated using various data and MC samples. The uncertainty for both the FC and the FV selection is 1%. The decay-electron rejection cut has errors of 0.2-0.4%, depending on neutrino flavor and interaction type. The uncertainties for the single electron-like ring selection and π^0 rejection are estimated by using the SK

atmospheric neutrino data and SK cosmic-ray muons. Electron-neutrino CC-enriched control samples based on these cuts were prepared, and the differences between MC predictions and data are used to extract the systematic uncertainty. The uncertainty associated with the π^0 background is determined by constructing a hybrid sample with either an electron-like ring taken from the atmospheric data sample or from decay-electrons selected in the stopping muon data sample, and a MC-generated gamma ray assuming π^0 kinematics. The selection cut systematic uncertainty is calculated to be 1.6% for signal events and 7.3% for background events. The total SK selection uncertainty is 2.1% for the ν_e candidate events assuming $\sin^2 2\theta_{13} = 0.1$.

Additional SK systematic uncertainties are due to final-state interactions (FSI) of pions that occur inside the target nucleus, as well as secondary interactions (SI) of pions and photo-nuclear (PN) interactions of photons that occur outside of the target nucleus. The treatment of the FSI and SI uncertainties is the same as in the previous analysis [28]. For this analysis, a new simulation of PN interactions has been added to the SK MC. In the final ν_e event sample, 15% of the remaining π^0 background is due to events where one of the π^0 decay photons is absorbed in a PN interaction. A systematic uncertainty of 100% is assumed for the normalization of the PN cross section.

Oscillation Analysis—The neutrino oscillation parameters are evaluated using a binned extended maximum-likelihood fit. The likelihood consists of four components: a normalization term ($\mathcal{L}_{\text{norm}}$), a term for the spectrum shape ($\mathcal{L}_{\text{shape}}$), a systematics term ($\mathcal{L}_{\text{syst}}$), and a constraint term ($\mathcal{L}_{\text{const}}$) from other measurements,

$$\mathcal{L}(N_{\text{obs}}, \vec{x}, \vec{\sigma}, \vec{f}) = \mathcal{L}_{\text{norm}}(N_{\text{obs}}; \vec{\sigma}, \vec{f}) \times \mathcal{L}_{\text{shape}}(\vec{x}; \vec{\sigma}, \vec{f}) \times \mathcal{L}_{\text{syst}}(\vec{f}) \times \mathcal{L}_{\text{const}}(\vec{\sigma}), \quad (3)$$

where N_{obs} is the number of observed events, \vec{x} is a set of kinematic variables, $\vec{\sigma}$ represents oscillation parameters, and \vec{f} describes systematic uncertainties. In the fit, the likelihood is integrated over the nuisance parameters to obtain a marginalized likelihood for the parameters of interest.

$\mathcal{L}_{\text{norm}}$ is calculated from a Poisson distribution using the mean value from the predicted number of MC events. $\mathcal{L}_{\text{syst}}(\vec{f})$ constrains the 27 systematic parameters from the ND280 fit, the SK-only cross section parameters, and the SK selection efficiencies. Table II shows the uncertainties on the predicted number of signal ν_e events. The $\mathcal{L}_{\text{shape}}$ term uses $x=(p_e, \theta_e)$ to distinguish the ν_e signal from backgrounds. An alternative analysis uses $x = E_\nu^{\text{rec}}$, the reconstructed neutrino energy. In order to combine the results presented in this letter with other measurements to better constrain $\sin^2 2\theta_{13}$ and δ_{CP} , the $\mathcal{L}_{\text{const}}$ term can also be used to apply additional constraints on $\sin^2 2\theta_{13}$, $\sin^2 \theta_{23}$ and Δm_{32}^2 .

TABLE II. The uncertainty (RMS/mean in %) on the predicted number of signal ν_e events for each group of systematic uncertainties for $\sin^2 2\theta_{13} = 0.1$ and 0. The uncorrelated ν interaction uncertainties are those coming from parts of the neutrino interaction model that cannot be constrained with ND280.

Error source [%]	$\sin^2 2\theta_{13} = 0.1$	$\sin^2 2\theta_{13} = 0$
Beam flux and near detector	2.9	4.8
(w/o ND280 constraint)	(25.9)	(21.7)
Uncorrelated ν interaction	7.5	6.8
Far detector and FSI+SI+PN	3.5	7.3
Total	8.8	11.1

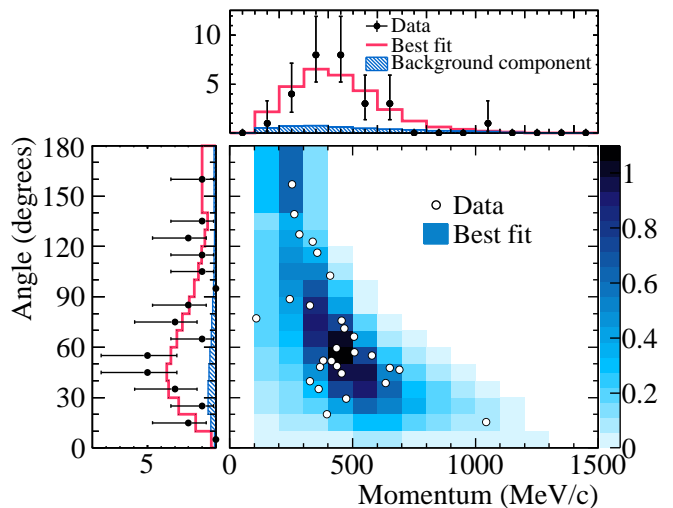


FIG. 3. The (p_e, θ_e) distribution for ν_e candidate events with the MC prediction using the primary method best-fit value of $\sin^2 2\theta_{13} = 0.140$ (normal hierarchy).

The following oscillation parameters are fixed in the analysis: $\sin^2 \theta_{12} = 0.306$, $\Delta m_{21}^2 = 7.6 \times 10^{-5} \text{ eV}^2$ [29], $\sin^2 \theta_{23} = 0.5$, $|\Delta m_{32}^2| = 2.4 \times 10^{-3} \text{ eV}^2$ [30] and $\delta_{\text{CP}} = 0$. For the normal (inverted) hierarchy case, the best-fit value with a 68% confidence level (CL) is $\sin^2 2\theta_{13} = 0.140^{+0.038}_{-0.032}$ ($0.170^{+0.045}_{-0.037}$). Figure 3 shows the best-fit result, with the 28 observed ν_e events. The alternative analysis using E_ν^{rec} and a profile likelihood method produces consistent best-fit values and nearly identical confidence regions. Figure 4 shows the E_ν^{rec} distribution with the MC prediction for the best-fit θ_{13} value in the alternative analysis.

The significance for a non-zero θ_{13} is calculated to be 7.3σ , using the difference of log likelihood values between the best-fit θ_{13} value and $\theta_{13} = 0$. An alternative method of calculating the significance, by generating a large number of toy MC experiments assuming $\theta_{13} = 0$, also returns a value of 7.3σ . These significances were calculated using a test statistic having fixed values for θ_{23} and δ_{CP} .

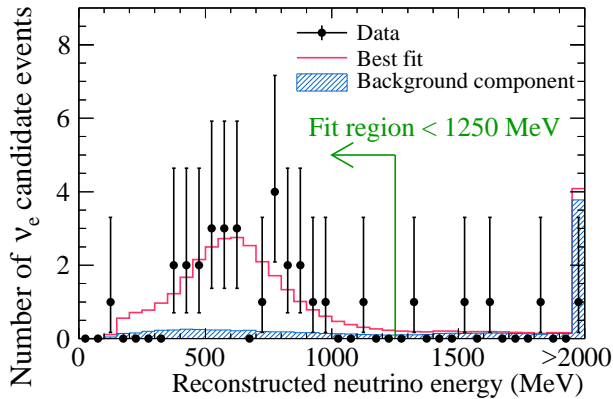


FIG. 4. The E_ν^{rec} distribution for ν_e candidate events with the MC prediction at the best fit of $\sin^2 2\theta_{13} = 0.144$ (normal hierarchy) by the alternative binned E_ν^{rec} analysis.

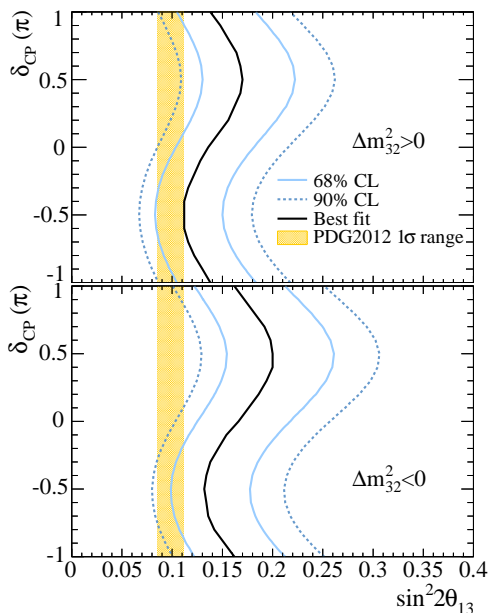


FIG. 5. The 68% and 90% CL allowed regions for $\sin^2 2\theta_{13}$, as a function of δ_{CP} assuming normal hierarchy (top) and inverted hierarchy (bottom). The solid line represents the best fit $\sin^2 2\theta_{13}$ value for given δ_{CP} values. The values of $\sin^2 \theta_{23}$ and Δm_{32}^2 are varied in the fit with the constraint from [30]. The shaded region shows the average θ_{13} value from the PDG2012 [8].

For any values for these parameters, consistent with their present uncertainties, the significance remains above 7σ .

As the precision of this measurement increases, the uncertainty from other oscillation parameters becomes increasingly important. The uncertainties on θ_{23} and Δm_{32}^2 are taken into account in the fit by adding a $\mathcal{L}_{\text{const}}$ term and marginalizing the likelihood over θ_{23} and Δm_{32}^2 . The $\mathcal{L}_{\text{const}}$ term is the likelihood as a function of $\sin^2 \theta_{23}$ and

Δm_{32}^2 , obtained from the T2K ν_μ disappearance measurement [30]. The value of δ_{CP} and the hierarchy are held fixed in the fit. Performing the fit for all values of δ_{CP} , the allowed 68% and 90% CL regions for $\sin^2 2\theta_{13}$ are obtained as shown in Figure 5. For $\delta_{\text{CP}} = 0$ and normal (inverted) hierarchy case, the best-fit value with a 68% CL is $\sin^2 2\theta_{13} = 0.136_{-0.033}^{+0.044}$ ($0.166_{-0.042}^{+0.051}$). With the current statistics, the correlation between the ν_μ disappearance and ν_e appearance measurements in T2K is negligibly small.

Constraints on δ_{CP} are obtained by combining our results with the θ_{13} value measured by reactor experiments. The additional likelihood constraint term on $\sin^2 2\theta_{13}$ is defined as $\exp\{-\frac{(\sin^2 2\theta_{13} - 0.098)^2}{2(0.013^2)}\}$, where 0.098 and 0.013 are the averaged value and the error of $\sin^2 2\theta_{13}$ from PDG2012 [8]. The $-2\Delta \ln \mathcal{L}$ curve as a function of δ_{CP} is shown in Figure 6, where the likelihood is marginalized over $\sin^2 2\theta_{13}$, $\sin^2 \theta_{23}$ and Δm_{32}^2 . The combined T2K and reactor measurements prefer $\delta_{\text{CP}} = -\pi/2$. The 90% CL limits shown in Figure 6 are evaluated by using the Feldman-Cousins method [31] in order to extract the excluded region. The data excludes δ_{CP} between 0.19π and 0.80π ($-\pi$ and -0.97π , and -0.04π and π) with normal (inverted) hierarchy at 90% CL.

The maximum value of $-2\Delta \ln \mathcal{L}$ is 3.38 (5.76) at $\delta_{\text{CP}} = \pi/2$ for normal (inverted) hierarchy case. This value is compared with a large number of toy MC experiments, generated assuming $\delta_{\text{CP}} = -\pi/2$, $\sin^2 2\theta_{13} = 0.1$, $\sin^2 \theta_{23} = 0.5$ and $\Delta m_{32}^2 = 2.4 \times 10^{-3} \text{ eV}^2$. The MC averaged value of $-2\Delta \ln \mathcal{L}$ at $\delta_{\text{CP}} = \pi/2$ is 2.20 (4.10) for normal (inverted) hierarchy case, and the probability of obtaining a value greater or equal to the observed value is 34.1% (33.4%). With the same MC settings, the expected 90% CL exclusion region is evaluated to be between 0.35π and 0.63π (0.09π and 0.90π) radians for normal (inverted) hierarchy case.

Conclusions—T2K has made the first observation of electron neutrino appearance in a muon neutrino beam with a peak energy of 0.6 GeV and a baseline of 295 km. With the fixed parameters $|\Delta m_{32}^2| = 2.4 \times 10^{-3} \text{ eV}^2$, $\sin^2 \theta_{23} = 0.5$, $\delta_{\text{CP}} = 0$, and $\Delta m_{32}^2 > 0$ ($\Delta m_{32}^2 < 0$), a best-fit value of $\sin^2 2\theta_{13} = 0.140_{-0.032}^{+0.038}$ ($0.170_{-0.037}^{+0.045}$) is obtained, with a significance of 7.3σ over the hypothesis of $\sin^2 2\theta_{13} = 0$. When combining the T2K result with the world average value of θ_{13} from reactor experiments, some values of δ_{CP} are disfavored at the 90% CL.

T2K will continue to take data to measure the neutrino oscillation parameters more precisely and to further explore CP violation in the lepton sector.

We thank the J-PARC staff for superb accelerator performance and the CERN NA61 collaboration for providing valuable particle production data. We acknowledge the support of MEXT, Japan; NSERC, NRC and CFI, Canada; CEA and CNRS/IN2P3, France; DFG, Germany; INFN, Italy; Ministry of Science and Higher Edu-

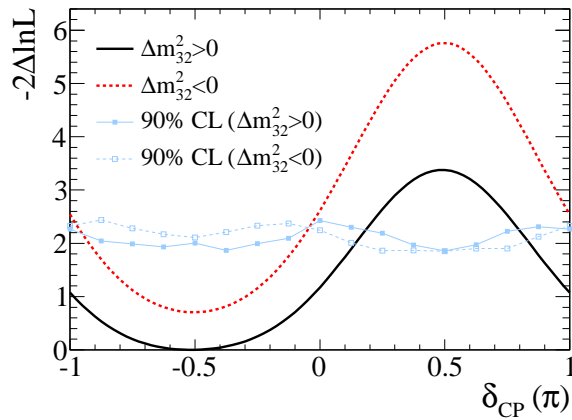


FIG. 6. The $-2\Delta \ln \mathcal{L}$ value as a function of δ_{CP} for normal hierarchy (solid line) and inverted hierarchy (dotted line). The likelihood is marginalized over $\sin^2 2\theta_{13}$, $\sin^2 \theta_{23}$ and Δm_{32}^2 . The solid (dotted) line with markers corresponds to the 90% CL limits for normal (inverted) hierarchy, evaluated by using the Feldman-Cousins method. The δ_{CP} regions with values above the lines are excluded at 90% CL.

cation, Poland; RAS, RFBR and MES, Russia; MICINN and CPAN, Spain; SNSF and SER, Switzerland; STFC, U.K.; and DOE, U.S.A. We also thank CERN for the UA1/NOMAD magnet, DESY for the HERA-B magnet mover system, NII for SINET4, the WestGrid and SciNet consortia in Compute Canada, and GridPP, UK. In addition participation of individual researchers and institutions has been further supported by funds from: ERC (FP7), EU; JSPS, Japan; Royal Society, UK; DOE Early Career program, U.S.A.

* also at J-PARC, Tokai, Japan

† also at Institute of Particle Physics, Canada

‡ affiliated member at Kavli IPMU (WPI), the University of Tokyo, Japan

§ also at Moscow Institute of Physics and Technology and National Research Nuclear University (MEPhI), Moscow, Russia

¶ also at JINR, Dubna, Russia

** deceased

†† also at BMCC/CUNY, Science Department, New York, New York, U.S.A.

- [1] Y. Fukuda *et al.* (Super-Kamiokande Collaboration), *Phys.Rev.Lett.* **81**, 1562 (1998).
 [2] K. Abe *et al.* (T2K Collaboration),

- Nucl.Instrum.Meth.* **A659**, 106 (2011).
 [3] K. Abe *et al.* (T2K Collaboration), *Phys.Rev.Lett.* **107**, 041801 (2011).
 [4] K. Abe *et al.* (T2K Collaboration), *Phys.Rev.* **D88**, 032002 (2013).
 [5] Z. Maki, M. Nakagawa, and S. Sakata, *Prog.Theor.Phys.* **28**, 870 (1962).
 [6] B. Pontecorvo, *Sov.Phys.JETP* **26**, 984 (1968).
 [7] M. Freund, *Phys.Rev.* **D64**, 053003 (2001).
 [8] J. Beringer *et al.* (Particle Data Group), *Phys.Rev.* **D86**, 010001 (2012).
 [9] F. An *et al.* (Daya Bay Collaboration), *Phys.Rev.Lett.* **108**, 171803 (2012).
 [10] J. Ahn *et al.* (RENO collaboration), *Phys.Rev.Lett.* **108**, 191802 (2012).
 [11] Y. Abe *et al.* (Double Chooz Collaboration), *Phys.Rev.Lett.* **108**, 131801 (2012).
 [12] P. Adamson *et al.* (MINOS Collaboration), *Phys.Rev.Lett.* **110**, 171801 (2013).
 [13] K. Abe *et al.* (T2K Collaboration), *Phys.Rev.* **D87**, 012001 (2013).
 [14] N. Abgrall *et al.* (NA61/SHINE Collaboration), *Phys.Rev.* **C84**, 034604 (2011).
 [15] N. Abgrall *et al.* (NA61/SHINE Collaboration), *Phys.Rev.* **C85**, 035210 (2012).
 [16] A. Ferrari, P. R. Sala, A. Fasso, and J. Ranft, CERN-2005-010, SLAC-R-773, INFN-TC-05-11.
 [17] G. Battistoni, S. Muraro, P. R. Sala, F. Cerutti, A. Ferrari, *et al.*, *AIP Conf.Proc.* **896**, 31 (2007).
 [18] R. Brun, F. Carminati, and S. Giani, CERN-W5013 (1994).
 [19] C. Zeitnitz and T. Gabriel, In *Corpus Christi 1992, Calorimetry in high energy physics* 394-404 (1992).
 [20] K. Abe *et al.* (T2K Collaboration), *Nucl.Instrum.Meth.* **A694**, 211 (2012).
 [21] Y. Hayato, *Acta Phys.Polon.* **B40**, 2477 (2009).
 [22] A. A. Aguilar-Arevalo *et al.* (MiniBooNE Collaboration), *Phys.Rev.* **D83**, 052009 (2011).
 [23] A. A. Aguilar-Arevalo *et al.* (MiniBooNE Collaboration), *Phys.Rev.* **D83**, 052007 (2011).
 [24] A. A. Aguilar-Arevalo *et al.* (MiniBooNE Collaboration), *Phys.Rev.* **D81**, 013005 (2010).
 [25] P. Amaudruz *et al.* (T2K ND280 FGD group), *Nucl.Instrum.Meth.* **A696**, 1 (2012).
 [26] N. Abgrall *et al.* (T2K ND280 TPC group), *Nucl.Instrum.Meth.* **A637**, 25 (2011).
 [27] R. B. Patterson *et al.*, *Nucl.Instrum.Meth.* **A608**, 206 (2009).
 [28] K. Abe *et al.* (T2K Collaboration), *Phys.Rev.* **D88**, 032002 (2013).
 [29] G. L. Fogli, E. Lisi, A. Marrone, A. Palazzo, and A. M. Rotunno, *Phys.Rev.* **D84**, 053007 (2011).
 [30] K. Abe *et al.* (T2K Collaboration), (2013), arXiv:1308.0465 [hep-ex].
 [31] G. J. Feldman and R. D. Cousins, *Phys.Rev.* **D57**, 3873 (1998).